

## **Supporting Information**

### **Reversible assembly-disassembly of plasmonic spherical nucleic acid enabling temperature-self-controllable and biomarker-activatable photothermal effect**

Lixian Huang, Jinling Zhang, Lifang Pang, Shengqiang Hu\*, Liangliang Zhang\*, and  
Shulin Zhao

State Key Laboratory for the Chemistry and Molecular Engineering of Medicinal  
Resources, School of Chemistry and Pharmaceutical Sciences, Guangxi Normal  
University, Guilin 541004, P. R. China

\*Corresponding author: zn\_sqhu@163.com (S.H.), liangzhang319@163.com (L.Z.).

## Materials and methods

**Materials.** Hydrogen tetrachloroaurate ( $\text{HAuCl}_4$ ), sodium citrate ( $\text{Na}_3\text{C}_6\text{H}_5\text{O}_7$ ), and tris(2-carboxyethyl)phosphine (TCEP) were purchased from Aladdin Co., Ltd. (Shanghai, China). Deoxyribonuclease-I (DNase-I) was acquired from Thermo Fisher Scientific Inc. (Waltham, MA, USA). Dimethyl sulfoxide (DMSO) and all of the oligonucleotides were provided by Sangon Biotech Co., Ltd. (Shanghai, China). Human breast carcinoma MCF-7 cells and human normal liver HL-7702 cells were obtained from Cobioer Biotech Co., Ltd. (Wuhan, China). Fetal bovine serum (FBS), phosphate buffered saline (PBS, pH = 7.4), Dulbecco's modified Eagle's medium (DMEM) cell culture medium, and thiazolyl blue tetrazolium bromide (MTT) were acquired from Beijing Soleub Technology Co., Ltd. (Beijing, China). BALB/c mice (6-8 weeks) were purchased from Hunan SLAC Laboratory Animal Co., Ltd. (Hunan, China), and all related experiments were performed in compliance with relevant laws or guidelines of China, followed institutional guidelines of China, and approved by the Institutional Ethical Committee (IEC) of Guangxi Normal University.

**Instrumentation.** Ultraviolet–visible (UV–vis) absorption spectra were collected on a Cary 60 spectrometer (Agilent, USA). The morphology and size of the gold nanoparticles were characterized with a transmission electron microscope (TEM, FEI, USA). The photothermal response of nanoassembly were performed under irradiation with a 660-nm laser (LASEVER, China), and the corresponding temperature change was monitored with an infrared imaging camera (Optris PI, Germany). Cell viability were measured using a microplate reader (BioTek instruments, USA). Cell imaging was conducted on a LSM-710 laser confocal microscope (ZEISS, Germany). The electrophoretic image was acquired with an Omega 16ic Gel imaging system (ULTRA-LUM, USA).

**Functionalization of AuNPs with DNA.** In general, AuNPs with a concentration of 13 nM were firstly synthesized according to a reported method.<sup>1</sup> Then, 5  $\mu\text{M}$

diblock and thiolated DNA was mixed with 13 nM AuNPs, respectively, followed by freezing at -20 °C for 2.0 h. After thawing at room temperature, free DNA was removed by centrifuging (13 000 rpm, 15 min) and washing with 10 mM PBS for three times. Finally, the obtained DNA functionalized AuNPs were dispersed in 10 mM PBS for further use. For thiolated DNA, an activation treatment was conducted with 2.2 mM TCEP at 37 °C for 0.5 h before use.

**Self-assembly of pSNAs.** Typically, A<sub>10</sub>P1 and A<sub>10</sub>P2 DNA were used for functional modification of AuNPs to prepare A<sub>10</sub>P1-pSNA and A<sub>10</sub>P2-pSNA, respectively. Then, 6.5 nM A<sub>10</sub>P1-pSNA and 6.5 nM A<sub>10</sub>P2-pSNA were mixed and incubated at 37 °C for 1.5 h. Finally, the formed nanoassembly were characterized using UV–vis absorption spectra and photothermal imaging. In some experiments, the sequence and amount of DNA were different.

**Nuclease stability assay of pSNAs.** Firstly, 6.5 nM A<sub>10</sub>P1-pSNA and 6.5 nM A<sub>10</sub>P2-pSNA were mixed and incubated at 37 °C for 1.5 h. Then, the formed nanoassembly were incubated with 0.5 and 1.0 U/mL DNase-I for 2.0 h, respectively, followed by photothermal and native polyacrylamide gel electrophoresis (PAGE) analysis.

**Cytotoxicity evaluation of pSNAs.** The cytotoxicity of pSNAs was assessed using MTT assay. Generally, 200 µL of fresh cell media containing different concentrations (0, 0.7, 6.5, 13 nM) of pSNAs were incubated with MCF-7 cells at 37 °C for 24.0 h, respectively. After washing with 10 mM PBS for three times, 200 µL of fresh cell media containing 20 µL of MTT (0.5 mg/mL) were added and incubated for another 4.0 h. Then, 200 µL of DMSO were added and shaken for 10 min to dissolve the formazan crystals. Finally, the absorbance intensity at 570 nm of the suspensions was measured on a microplate reader. The cell viability was calculated based on the percent absorbance of pSNAs-treated group relative to that of PBS-treated one.

**DNA-21-activatable photothermal effect *in vitro*.** In brief, different

concentrations (0, 5, 10, 25, 100 nM) of DNA-21 was added into 6.5 nM pSNAs solution (the mixture of H1-pSNA and H2-pSNA). After incubation at 37 °C for 2.0 h, the resulting nanoassembly was irradiated with a 660-nm laser for 10 min, and the solution temperature was recorded with an infrared imaging camera. The selectivity assay was carried out with other DNAs including Mismatch-1, DNA-223, DNA-141, DNA-26, and DNA-16.

**Selective photothermal cytotoxicity of pSNAs *in vitro*.** Briefly, 200  $\mu$ L of fresh cell media containing 10 mM PBS or 6.5 nM pSNAs were incubated with MCF-7, HL-7702 cells at 37 °C for 24.0 h, respectively. After washing with 10 mM PBS for three times, the cells were irradiated with a 660-nm laser (1.5 W/cm<sup>2</sup>) for 10 min. Then, 200  $\mu$ L of fresh cell media were added and incubated for another 8 h. Finally, the cells were treated with MTT for quantitative detection of cell viability, or incubated with 5  $\mu$ L of calcein-AM and PI for the imaging-based analysis of cell state.

**Serve and activatable photothermal performance *in vivo*.** The suspensions of human breast carcinoma MCF-7 cells (100  $\mu$ L,  $5 \times 10^6$  cells) were subcutaneously injected to the hind limb of mouse. Once the tumor size reached about 100 mm<sup>3</sup>, the mice was divided into three groups and intravenously injected with 10 mM PBS, 13 nM pSNAs, and nanoassembly (13 nM pSNAs + 50 nM DNA-21), respectively. After 2.0 h, the tumor region was irradiated with a 660-nm laser for 10 min and imaged with an infrared imaging camera.

**Table 1.** DNA sequences used in this work

Name	Sequence (from 5' to 3')
R-A <sub>30</sub>	GAT TTT GAG TTTT AAAAA AAAAA AAAAA AAAAA AAAAA AAAAA
R-A <sub>15</sub>	GAT TTT GAG TTTT AAAAA AAAAA AAAAA
A <sub>10</sub> P1 (R-A <sub>10</sub> )	GAT TTT GAG TTTT AAAAA AAAAA
L-A <sub>30</sub>	CTC AAA ATC TTTT AAAAA AAAAA AAAAA AAAAA AAAAA AAAAA
L-A <sub>15</sub>	CTC AAA ATC TTTT AAAAA AAAAA AAAAA
A <sub>10</sub> P2 (L-A <sub>10</sub> )	CTC AAA ATC TTTT AAAAA AAAAA
R-T <sub>10</sub>	GAT TTT GAG TTTT TTTT-SH
R-T <sub>15</sub>	GAT TTT GAG TTTT TTTT TTTT-SH
R-T <sub>30</sub>	GAT TTT GAG TTTT TTTT TTTT TTTT TTTT TTTT-SH
L-T <sub>10</sub>	CTC AAA ATC TTTT TTTT-SH
L-T <sub>15</sub>	CTC AAA ATC TTTT TTTT TTTT-SH
L-T <sub>30</sub>	CTC AAA ATC TTTT TTTT TTTT TTTT TTTT TTTT-SH
P1 (R-T <sub>5</sub> )	GAT TTT GAG TTTT-SH
P3	CTC CAG CTG TTTT-SH
P5	CAC AGA CAG TTTT-SH
P2 (L-T <sub>5</sub> )	CTC AAA ATC TTTT-SH
P4	CAG CAG GAG TTTT-SH
P6	CTG TCT GTG TTTT-SH
H1	HS-TTTT TTTT TCA ACA TCA GTC TGA TAA GCT ACC ATG TGT AGA TAG CTT ATC AGA CT
H2	HS-TTTT TTTT ATA AGC TAT CTA CAC ATG GTA GCT TAT CAG ACT GAT GCC ATG TGT AGA
DNA-21	TAG CTT ATC AGA CTG ATG TTG A
Mismatch-1	TAG CTT ATC AGT CTG ATG TTG A
DNA-223	TGT CAG TTT GTC AAA TAC CCC A
DNA-141	TAA CAC TGT CTG GTA AAG ATG G
DNA-26	TTC AAG TAA TCC AGG ATA GGC T
DNA-16	TAG CAG CAC GTA AAT ATT GGC G

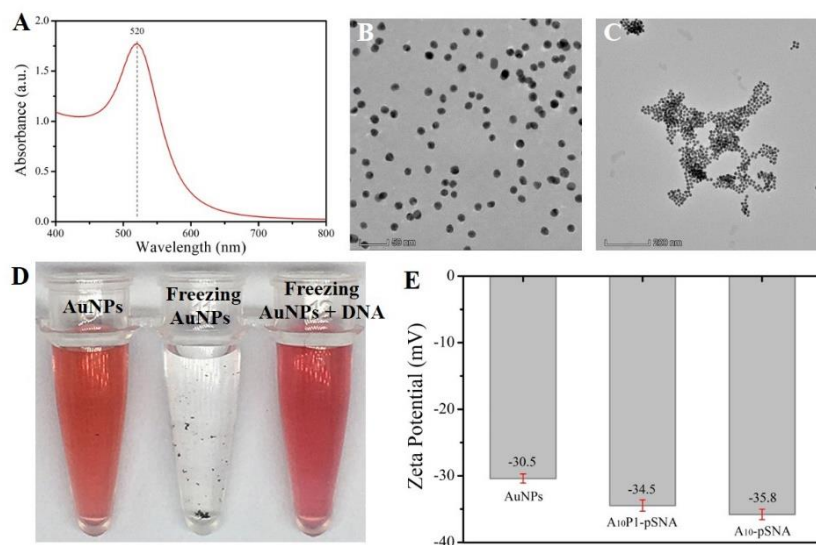


**Fig. S1** (A) UV-vis absorption spectrum of AuNPs. TEM images of (B) AuNPs and (C) nanoassembly of A<sub>10</sub>P1-pSNA and A<sub>10</sub>P2-pSNA. (D) Photographs of AuNPs before and after a freeze-thaw process in the absence and presence of A<sub>10</sub>P1 DNA. (E) Zeta potential characterization of functional modification of AuNPs with DNA.

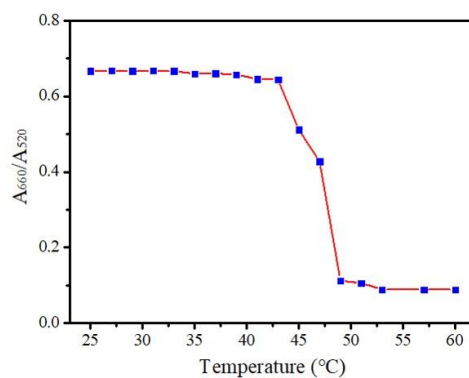


**Fig. S2** Melting temperature curve of the nanoassembly formed by the incubation of 6.5 nM A<sub>10</sub>P1-pSNA with 6.5 nM A<sub>10</sub>P2-pSNA.

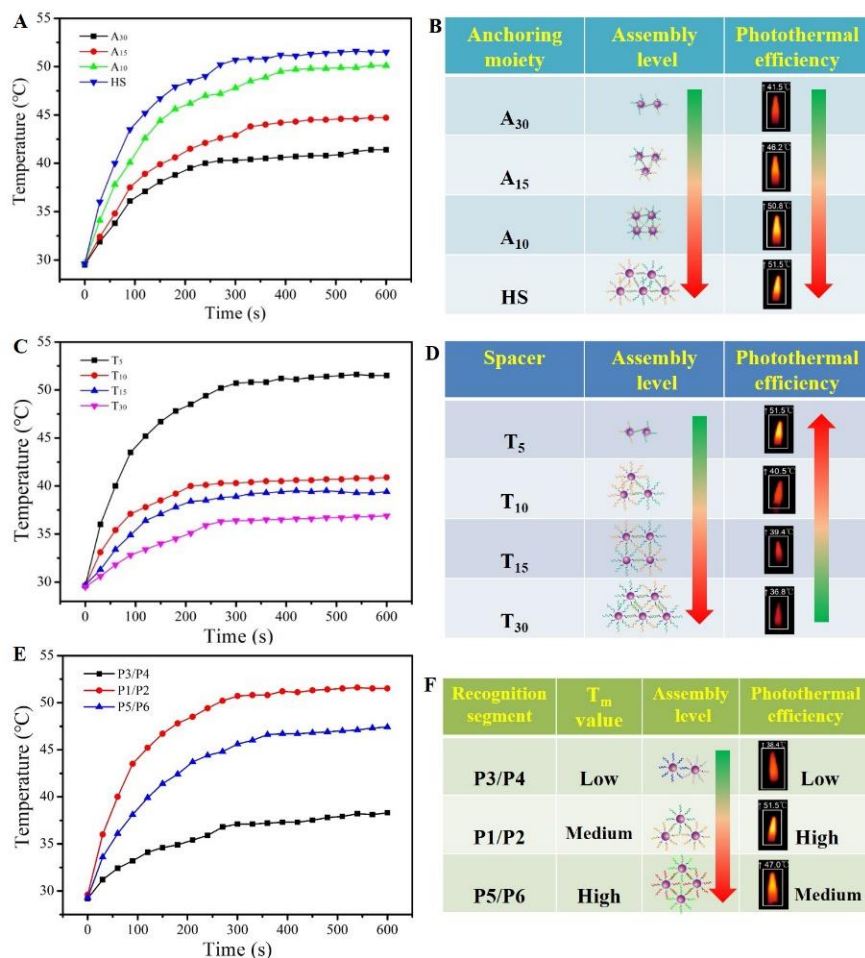


**Fig. S3** The effect of the anchoring moiety (A, B), spacer (C, D) and recognition segment (E, F) of DNA on the self-assembly and photothermal efficiency of pSNAs.

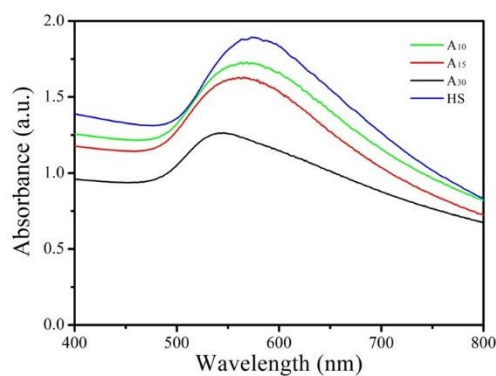


**Fig. S4** UV-vis spectrum of the nanoassembly as a function of the anchoring moiety of DNA.

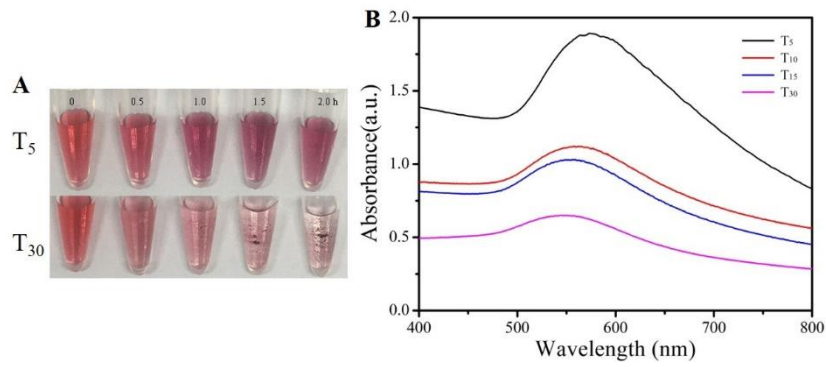


**Fig. S5** (A) Comparison of self-assembly efficiency between the samples of T<sub>5</sub> spacer and T<sub>30</sub> spacer, respectively. (B) UV-vis spectrum of the nanoassembly as a function of DNA spacer.

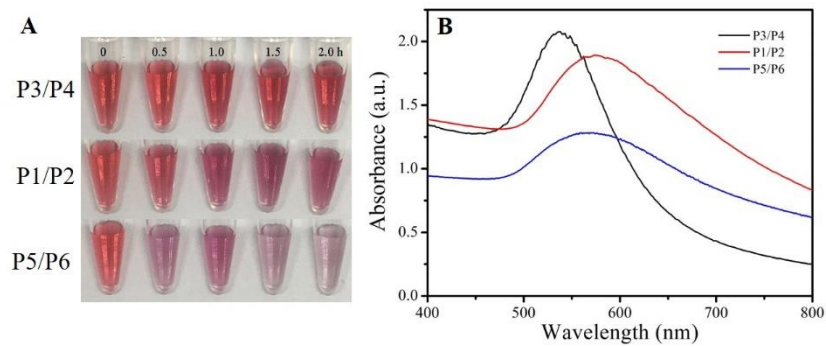


**Fig. S6** (A) Comparison of self-assembly efficiency among the samples with different recognition segments, respectively. (B) UV-vis spectrum of the nanoassembly as a function of recognition segment of DNA.

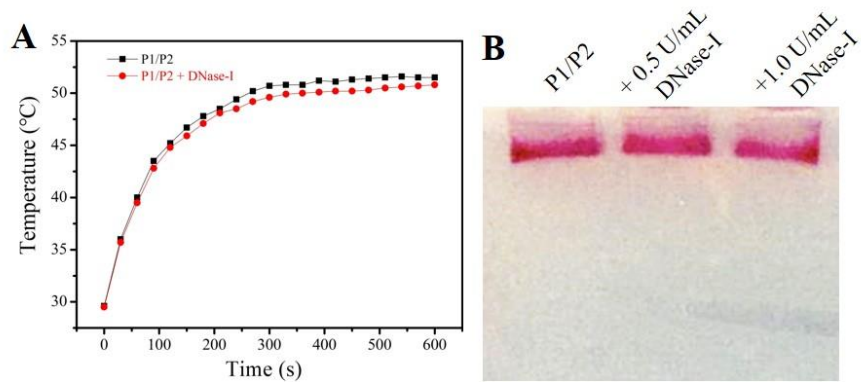


**Fig. S7** (A) Photothermal and (B) native PAGE analysis of the nuclease stability of P1/P2-pSNAs after treatment with deoxyribonuclease-I (DNase-I).

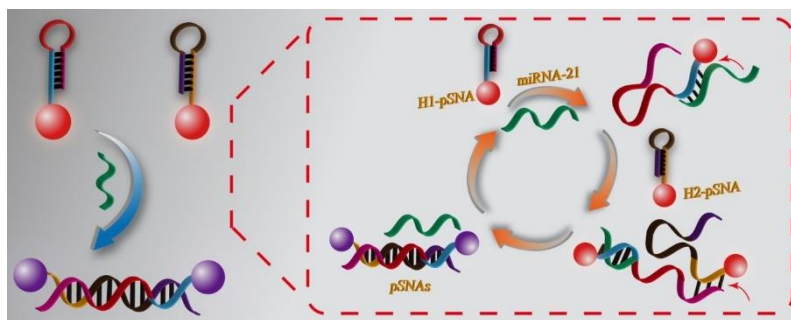


**Fig. S8** Schematic illustration of CHA-mediated amplified self-assembly of pSNAs.

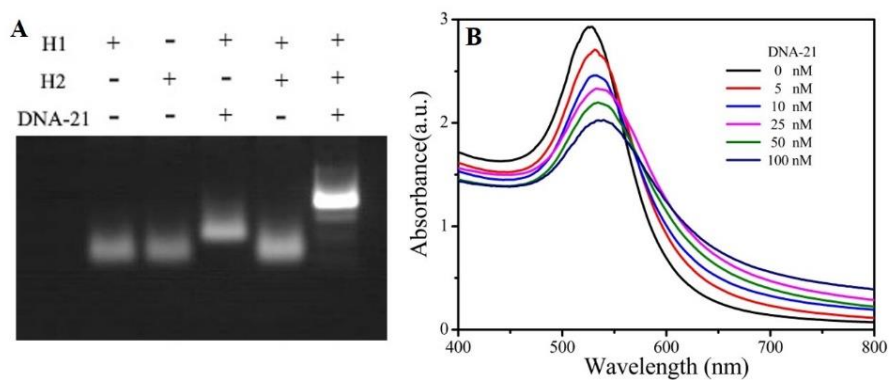


**Fig. S9** (A) Native PAGE analysis of CHA reaction. (B) UV-vis spectrum of pSNAs-CHA system in the presence of different concentrations of DNA-21.

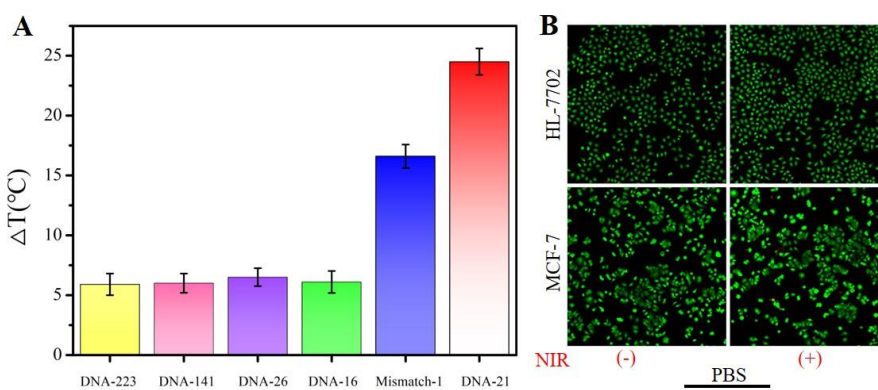


**Fig. S10** (A) Selectivity assay for DNA-21 detection. (B) Fluorescence images of HL-7702 and MCF-7 cells after PBS treatment.

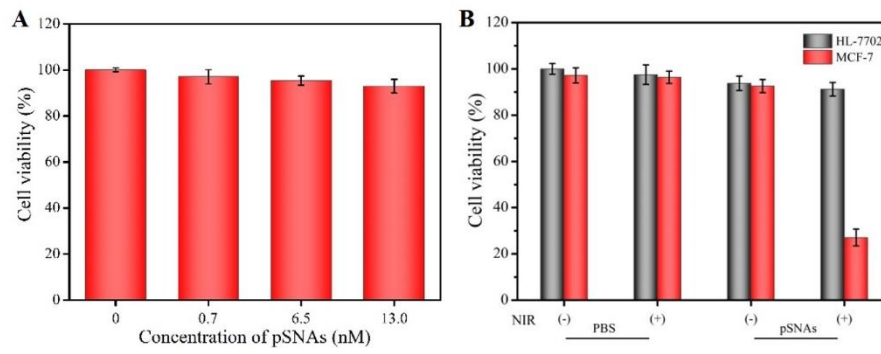


**Fig. S11** (A) Cytotoxicity of pSNAs. (B) Cell viability of HL-7702 and MCF-7 cells after different treatments.

### **Additional reference**

1. J. Liu, Y. Lu, *Nat. Protoc.* 2006, **1**, 246-252.